Multi-Frame Blind Deconvolution for Imaging in Daylight and Strong Turbulence Conditions

Michael Hart, Stuart Jefferies, Douglas Hope, and E. Keith Hege
HartSCI LLC, 5434 E. Burns St., Tucson, AZ 85711

Runa Briguglio, Enrico Pinna, Alfio Puglisi, Fernando Quiros, and Marco Xompero
Osservatorio Astrofisico di Arcetri, Largo Enrico Fermi 5, 50125 Firenze, Italy

ABSTRACT

We describe results from new computational techniques to extend the reach of large ground-based optical telescopes, enabling high resolution imaging of space objects under daylight conditions. Current state-of-the-art systems, even those employing adaptive optics, dramatically underperform in such conditions because of strong turbulence generated by diurnal solar heating of the atmosphere, characterized by a ratio of telescope diameter to Fried parameter as high as 70. Our approach extends previous advances in multi-frame blind deconvolution (MFBD) by exploiting measurements from a wavefront sensor recorded simultaneously with high-cadence image data. We describe early results with the new algorithm which may be used with seeing-limited image data or as an adjunct to partial compensation with adaptive optics to restore imaging to the diffraction limit even under the extreme observing conditions found in daylight.

Keywords: Multi-frame blind deconvolution, daylight observing

1. BACKGROUND AND MOTIVATION

Imaging from ground-based telescopes is challenged by blurring caused by seeing, the random and rapidly varying optical aberration introduced by the atmosphere. As a consequence, while the resolving power of a telescope is in principle set by the physical size of the entrance aperture and the wavelength of observation, in practice, image resolution is reduced by an order of magnitude or more by atmospheric turbulence.

Ground-based observations of space objects made with passive imaging systems must rely either on reflected sunlight or the object's intrinsic thermal radiation. The latter, peaking in brightness between 5 and 10 μm, can only provide images of restricted resolution because of the long wavelength. Visible light imaging systems can deliver significantly better resolving power for the same aperture size. However, to overcome atmospheric seeing and achieve the theoretical limit of image sharpness requires the use of both adaptive optics (AO) to correct aberrations before detection and image post-processing to redistribute recorded flux after detection. Unfortunately, both adaptive optics and numerical image restoration techniques become rapidly more challenging as the aberrations increase in strength. This happens as observations are made at shorter wavelengths, with larger apertures, or as the seeing worsens.

A key parameter that characterizes the strength of image blurring caused by seeing is D/r_0 where D is the telescope diameter and r_0 is the Fried scale, or atmospheric coherence length. Present AO and post-processing image restoration techniques work well in the regime $D/r_0 < \sim 20$. High-resolution observations of space objects at visible wavelengths may therefore be made with telescopes of 3–4 m diameter at night, when r_0 at a good mountaintop site is on the order of 15–20 cm. However, during the night, space objects in low earth orbit (LEO) are typically obscured by the earth's shadow except at dawn and dusk when the object is sunlit and the telescope is still in the dark. Presently, high-resolution observations of LEO space objects that rely on reflected sunlight are restricted to this so-called 'terminator mode' which limits the periods of time within which a particular object may be observed. The restriction could be lifted if high-resolution observations could be made in full daylight.

To realize that goal, two challenges must be overcome. First is the bright background of Rayleigh-scattered sunlight from the sky. Second is the substantially worse seeing that arises because the air within the first few hundred meters of the ground is heated by re-radiated solar energy. Even at a good observatory site, daytime seeing of 3–4 arc sec is not unusual, leading to D/r_0 values of 50 to 70. In this regime neither adaptive optics nor previously existing numerical image compensation techniques have adequate traction. In this paper we describe results from a new algorithm, based on the technique of multi-frame blind deconvolution (MFBD), that is able to recover high quality images of space objects from high-cadence short exposure images in seeing conditions of D/r_0=70, going well beyond the present state of the art.

Unconventional Imaging, Wavefront Sensing, and Adaptive Coded Aperture Imaging and Non-Imaging Sensor Systems, edited by Jean J. Dolne, Thomas J. Karr, Victor L. Gamiz, Stanley Rogers, David P. Casasent, Proc. of SPIE Vol. 8165, 81650L · © 2011 SPIE · CCC code: 0277-786X/11/$18 · doi: 10.1117/12.896564

2. NATURE OF THE CHALLENGE

We are concerned about two key physical effects that challenge MFBD at this extreme level of turbulence, beyond the fact of the atmospheric aberration itself. These are the polychromatic nature of the imaging, and the photon noise attributable to the object as well as introduced by the background brightness of the daytime sky. The reason why the broad optical bandwidth is of greater concern here than in more moderate seeing is that the radial smearing, which results in the loss of high-frequency information in the speckle structure, increases linearly with angular distance from the optical axis. Because extreme seeing throws energy to greater angular distances within the PSF, the effect is worse. At the same time, the greater field of view required to capture the complete broadly smeared image results in more bright daytime background light being included in the MFBD restorations, with concomitant increase in photon noise from scattered sunlight. Furthermore, because different regions of a resolved object are now mixed together across a wider angular extent in the raw image by the very blurry PSF, photon noise from the object makes it very much more challenging to deconvolve the PSF accurately.

Fundamentally, the purpose of MFBD is to separate each observation into estimates of the object and a PSF. A further challenge to this task arises in the fact that as the optical aberration increases, not only must the low spatial frequencies of the two be estimated to higher accuracy by MFBD, but a greater fraction of the high spatial frequency content must be estimated as well. Whereas a large fraction of the PSF energy is concentrated in a few well-defined "dominant" speckles at low D/r_0 values, which provide a good lever for MFBD algorithms, since most of the energy is contained in a few displaced copies of the object, this is not true at high D/r_0 values. Here there are many speckles of similar amplitudes and the energy of the PSF is spread out over a greater spatial extent (i.e. there are many displaced copies of the target with similar brightness). Furthermore, whereas the positions of the dominant speckles at low D/r_0 values are relatively insensitive to the high spatial frequencies in the wavefront phase, the converse is true at high D/r_0 values. In this regime, small perturbations in the high spatial frequencies can result in large changes in the speckle morphology.

Real observing conditions impose a finite signal-to-noise ratio (SNR). Inevitably then, there will be some value of D/r_0 above which all MFBD techniques will fail *unless supplemented with additional information on the high spatial frequencies of the wavefront phase*. This is especially true when the object under observation has a compact spectrum (i.e. the object is large with few highly detailed features) which reduces the amplitude of the observed high frequency content in the image. To extend the basic concept of MFBD to the extreme seeing conditions pertaining in daylight even at a good site therefore requires information about the problem that is not normally included in the restoration process. In these conditions the space of all conceivable solutions becomes so large that a search for the right solution in any given case is impractical without the additional information to constrain the search.

3. APPROACH

Our approach then has been to augment the normal high-cadence image data required by MFBD algorithms with simultaneous data from a wavefront sensor (WFS). We assume that the object to be observed is itself used as well to provide the wavefront data from a Shack-Hartmann sensor. The output of the WFS is simply recorded, not used to drive an AO system.

We exploit temporal correlations in the WFS data through the frozen flow hypothesis (FFH) which assumes that the turbulence can be modeled by a series of independent static layers, each moving across the telescope aperture with the prevailing wind at the altitude of the layer. Because of its simplicity, the FFH is frequently used as the basis for numerical studies of telescope imaging performance, particularly in the modeling of AO systems. While the FFH is observed not to hold in the real world over long time scales, a number of studies[1–3] have shown that it is a reasonable approximation for short but still interesting periods. For example, from observations made at the 1.5 m telescope of the Starfire Optical Range in New Mexico, at 0.74 μm wavelength, Schöck & Spillar [ref. 3] found that the FFH is accurate for time scales $\tau_{FFH} \sim 20$ ms or less. The accuracy degraded with increasing time such that by ~100 ms only 50% of the temporal evolution of the wave front could be described by the FFH. We note that their measurements were obtained under strong turbulence conditions, characterized by $D/r_0 \sim 40$.

The relevant time scale for comparison is τ_0, the expectation value of the time required for the phase of a wave front in a circular telescope aperture to change by 1 radian rms.[4] Values of τ_0 for observations at visible wavelengths are typically 1-3 ms depending on the quality of the site. For a single layer with Kolmogorov turbulence statistics and moving with local wind speed v, $\tau_0 = 0.31 r_0/v$.[5] Extending the idea from a single layer to the full depth of the atmosphere, the overall

atmospheric coherence time is $0.31r_0/\langle v \rangle$ where $\langle v \rangle$ is the mean wind speed integrated vertically through the atmosphere and weighted by the C_n^2 profile.[6] Of importance for any method that seeks to estimate an object by deconvolving the atmospheric point-spread function (PSF) from an image, τ_0 is also the period over which the PSF is approximately constant and so sets an effective upper limit to the imaging camera's exposure time.

Critically for the present study, we note that the period of validity of the FFH, τ_{FFH}, is an order of magnitude longer than τ_0. As a consequence, we may expect that the temporal correlation seen in a series of roughly 10 consecutive short-exposure images, each of integration time $\sim\tau_0$, will be well modeled by the effects of an atmosphere comprising a number of stacked layers, each propagating with its own wind vector, but otherwise unchanging. The FFH has been studied for use in AO to overcome system lag by predicting atmospheric turbulence a few milliseconds in advance,[7,8] but to the best of our knowledge it has not been used in image post processing to capture the inherent temporal correlations that exist in high-cadence imagery of targets observed through atmospheric turbulence.

4. VALIDATION OF WAVEFRONT ESTIMATION

An important element of our approach is to supplement the high-cadence image data with simultaneous and synchronized WFS data.[9] The purpose is to enable independent estimates of the frame-by-frame PSFs in order to provide a high quality start for the MFBD object restoration. Of course, wavefront reconstruction from WFS data is a standard and fundamental feature of every AO system in operation, and from the reconstructions, corresponding PSFs may be estimated. However, that approach is band-limited to spatial frequencies in the wavefront no higher than twice the spacing of subapertures in the WFS. In conventional night-time imaging at visible wavelengths, aberration on scales of a few centimeters (an order of magnitude smaller than r_0) can generally be ignored even by high-order AO systems correcting to the diffraction limit. For regimes of high D/r_0 such spatial scales become critical; but to sense them adequately one would typically require a WFS with so many subapertures that the signal-to-noise ratio in each would be unworkably small. Instead, our algorithm assumes the presence of a WFS of moderate order and adopts the FFH, taking advantage of the temporal correlations in the wavefront to sample on much finer scales than the individual subapertures. A joint estimation of all the wavefronts in a continuous sequence of frames is computed simultaneously from the corresponding sequence of WFS data. In addition, by adopting the FFH we reduce the number of variables required to characterize the imaging problem. This is valuable in that it reduces the required MFBD computation time (both the time per iteration and the number of iterations needed), and also because it improves the robustness of the algorithm by reducing the density of local minima.

A key question then is the accuracy with which the aberrated wavefronts in the telescope pupil can be recovered from the WFS measurements. This is hard to assess from simulations of the atmosphere because numerical models are generally inadequate in their implementation of the C_n^2 profile and the temporal statistics of the aberration above second order. We have therefore tested the method on real wavefront data acquired from the first-light AO system now running on the Large Binocular Telescope (LBT).[10,11] The LBT features two 8.4 m diameter primary mirrors on a common mount. The AO system runs at 989 Hz update rate and telemetry from the system may be collected at 300 Hz. We have used real-time closed-loop deformable mirror command data to obtain high-quality estimates of the open-loop wavefronts over one of the primary mirrors.[12]

Figure 1 (left hand column) shows the first and last frames of a continuous 30-frame (0.9 s) sequence of these deformable mirror commands. These shapes accurately reflect the true instantaneous atmospheric aberration; concurrent long-exposure images of the guide star showed a Strehl ratio consistent with total residual wavefront error of just 95 nm, including fitting error. Wavefront sensor slopes corresponding to these 'true' wavefronts, calculated on a Shack-Hartmann sensor of 30×30 subapertures, were analyzed by our algorithm assuming a turbulence model comprising two atmospheric layers moving according to the FFH. The estimated wavefronts (Figure 1, right hand column) accurately reflect the true wavefronts. The result confirms that this critical piece of our algorithm is indeed capable of extending beyond the realm of simulation and can operate successfully with real telescope data.

5. RESULTS

Tests of the new restoration algorithm have been carried out with simulated data in daylight conditions of background and poor seeing. Aberrated PSFs in a continuous sequence of 256 frames were made for the study using the parameters given in Table 1. Figure 2 shows four consecutive examples for a point source of magnitude 6 in the astronomical I band around 750 nm wavelength. The assumed filter profile is shown in Figure 3.

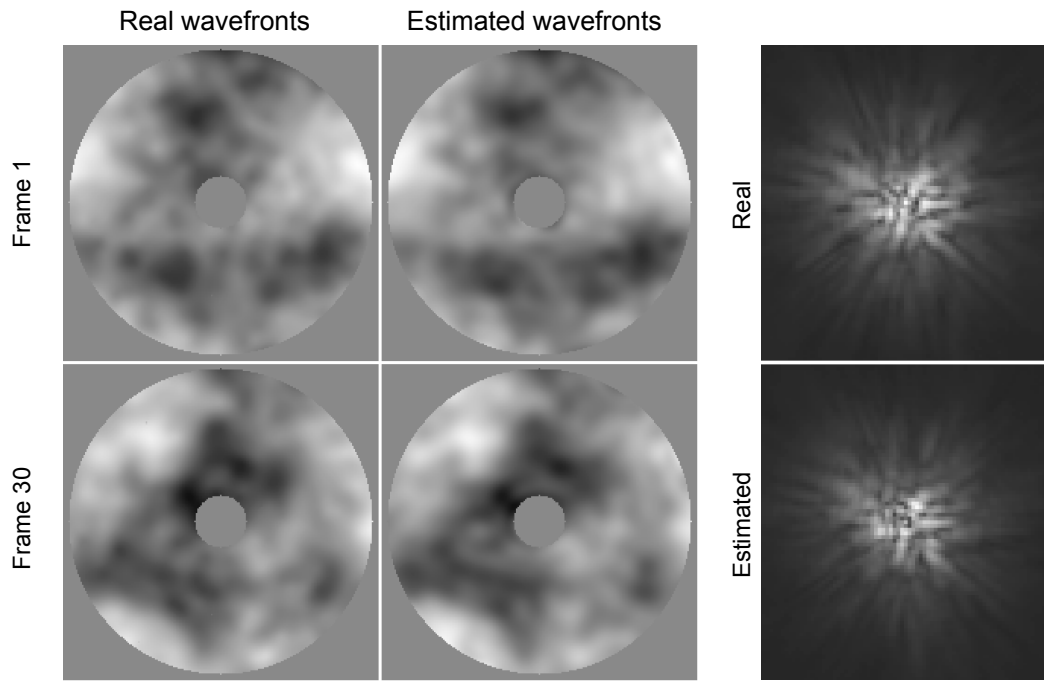

Figure 1. Wavefront estimation applied to real wavefronts recorded at the 8.4 m Large Binocular Telescope. (*Right*) Polychromatic PSFs calculated from a real wavefront and the corresponding estimated wavefront.

Table 1. Parameters for the simulated PSFs used in the study.

Parameter	**Value**
Aperture diameter	3.6 m
Mean wavelength	744 nm
Optical bandwidth	40%
Exposure time	4 ms
r_0 (744 nm)	5.2 cm
Seeing (744 nm)	2.9 arcsec
Stellar flux ($m_I = 6$)	5.3×10^7 photon/m^2/s
Sky background	2.1×10^7 photon/m^2/s/sq. arcsec
Solar elongation	70º

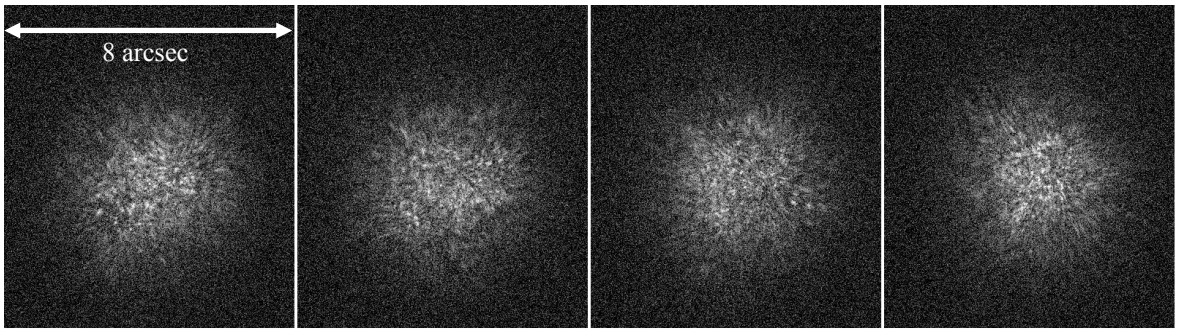

Figure 2. Example simulated PSFs from a 3.6 m telescope at $D/r_0 = 70$ using the parameters of Table 1. These PSFs include photon noise appropriate for a star of apparent I magnitude 6 and sky background for a daytime solar elongation of 70º.

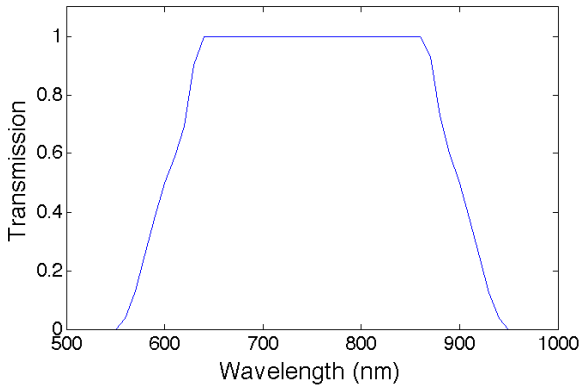

Figure 3. Assumed transmission for the filter used to generate polychromatic image data.

In Figure 4 we illustrate the success of our approach using simultaneous WFS data. Here we show the result of a complete end-to-end simulation in which a restored image is recovered from just 120 ms of data in 30 frames of 4 ms exposure time. The target was taken to have visual magnitude 4, observed 60 degrees away from the sun through turbulence conditions of $D/r_0 = 70$, corresponding to seeing of 3 arc sec at a 3.6 m telescope. The simulation included a multi-layer turbulent atmosphere, with polychromatic imaging across the full band from 600–900 nm wavelength.

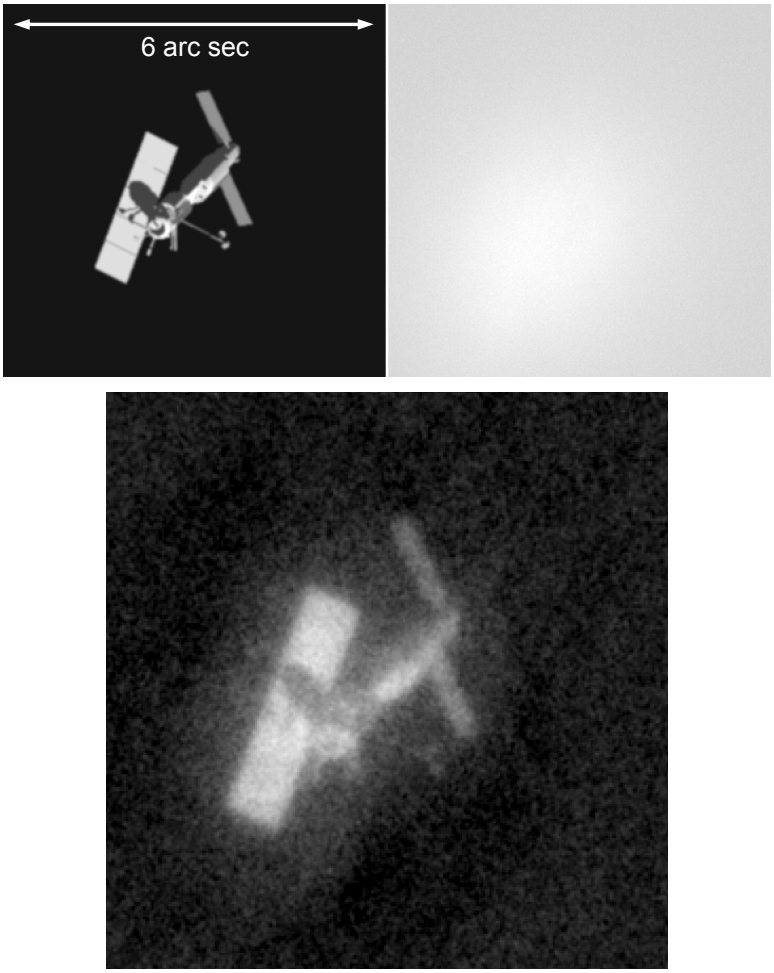

Figure 4. Result of image restoration at $D/r_0 = 70$ under daylight conditions. (*Left*) Pristine object; (*center*) single 4 ms snapshot; (*right*) restored object estimate.

Photon noise has been included in both the image data (Figure 4 center) and the WFS data, which also take into account the loss of sensitivity caused by the resolved nature of the object. The photon flux in these simulations has been calibrated against actual daylight image data, and therefore realistically accounts for the losses to be expected in a real optical system. We note that the central panel of Figure 4 is shown on a linear gray scale that starts at zero: the figure reflects the bright sky background against which the object must be observed.

6. CONCLUSION

We have demonstrated a breakthrough in the restoration of high quality object estimates from severely degraded imagery recorded under conditions of strong atmospheric turbulence and shot noise from a bright background. This is enabled through the use of an adjunct data stream along with the direct image data that assists in characterizing the instantaneous nature of the blurring. In addition to the WFS data, our method benefits from modeling the temporal correlations in the wavefront phases over short time intervals by using the FFH during the image restoration process. The FFH reduces variable count and allows for an effective sub-sampling of the wavefront phase that facilitates the reconstruction of the high spatial frequencies in the phase that are not sampled by the subapertures in the WFS. This property allows us to extend the range of imaging conditions over which high-quality restorations can be obtained into the regime where r_0 is less than the subaperture spacing, and where AO compensation loses its effectiveness. This enables high-Strehl imaging at shorter wavelengths and in stronger turbulence than has hitherto been possible. We note the additional sampling afforded by the FFH should also help in the reconstruction of the wavefront when observing in extremely low light conditions where photons may not be captured by every sub-aperture.

ACKNOWLEDGEMENTS

This work has been support by the Air Force Research Laboratory under contract number FA9451-11-M-0026. We are grateful to the AO teams of the LBT and the Arcetri Astrophysical Observatory for the data used in Section 4.

REFERENCES

[1] Poyneer, L. A., van Dam, M. and Véran, J.-P., "Experimental verification of the frozen flow atmospheric turbulence assumption with use of astronomical adaptive optics telemetry," J. Opt. Soc. Am. A **26**, 833 (2009).

[2] Schöck M. and Spillar, E. J., "Method for a quantitative investigation of the frozen flow hypothesis," J. Opt. Soc. Am. A **17**, 1650–1658 (2000).

[3] Gendron E. and Léna, P., "Single layer atmospheric turbulence demonstrated by adaptive optics observations," Astrophys. Space Sci. **239**, 221–228 (1996).

[4] Fried, D. L. "Time-delay-induced mean-square error in adaptive optics," J. Opt. Soc. Am. A **7**, 1224-1225 (1990).

[5] Buscher, D. F., Armstrong, J. T., Hummel, C. A., Quirrenbach, A., Mozurkewich, D., Johnston, K. J., Denison, C. S., Colavita, M. M. and Shao, M., "Interferometric seeing measurements on Mt. Wilson: power spectra and outer scales," App. Opt. **34**, 1081–1096 (1995).

[6] Hardy, J. W., "Adaptive optics for astronomical telescopes," Oxford Series in Optical and Imaging Science, Oxford University Press, §9.4.3 (1998)

[7] Page, K. A., "Exploiting the frozen flow hypothesis for linear predictions in adaptive optics," presented in Session 145 on Astronomical Instruments and Analytical Tools at the AAS 199th meeting, Washington DC, Jan 10, (2002).

[8] Poyneer, L. A., Macintosh, B. A. and Véran, J.-P., "Fourier transform wavefront control with adaptive prediction of the atmosphere," J. Opt. Soc. Am. A **24**, 2645-2660 (2007).

[9] Jefferies, S. M. and Hart, M., "Deconvolution from wave front sensing using the frozen flow hypothesis," Opt. Exp. **19**, 1975–1984 (2011).

[10] Esposito, S. et al., "First light AO (FLAO) system for LBT: final integration, acceptance test in Europe, and preliminary on-sky commissioning results," in Adaptive Optics Systems II (Proc. SPIE), eds. B. L. Ellerbroek, M. Hart, N. Hubin, & P. L. Wizinowich, **7736**, 773609 (2010).

[11] Riccardi, A. et al., "The adaptive secondary mirror for the Large Binocular Telescope: optical acceptance test and preliminary on-sky commissioning results," in Adaptive Optics Systems II (Proc. SPIE), eds. B. L. Ellerbroek, M. Hart, N. Hubin, & P. L. Wizinowich, **7736**, 77362C (2010).

[12] Hart, M., Briguglio, R., Pinna, E., Puglisi, A., Quiros, F., and Xompero, M., "Linear estimation of the Giant Magellan Telescope inter-segment optical path error from deformable mirror commands," Opt. Exp. submitted.